JNeurosci
THE JOURNAL OF NEUROSCIENCE

Gaze-stabilizing central vestibular neurons project asymmetrically to extraocular motoneuron pools

David Schoppik[1], Isaac H. Bianco[2], David A. Prober[3], Adam D. Douglass[4], Drew N. Robson[5], Jennifer M.B. Li[5], Joel S.F. Greenwood[6], Edward Soucy[7], Florian Engert[7,8] and Alexander F. Schier[7,8]

[1]Departments of Otolaryngology, Neuroscience & Physiology, and the Neuroscience Institute, New York University School of Medicine, New York, NY 10016

[2]Department of Neuroscience, Physiology and Pharmacology, University College London WCE1 6BT England

[3]Division of Biology, Caltech, Pasadena CA 91125

[4]Department of Neurobiology and Anatomy, University of Utah, Salt Lake City UT 84132

[5]Rowland Institute at Harvard, Cambridge MA 02142

[6]Department of Neuroscience, Yale University School of Medicine, New Haven CT 06510

[7]Center for Brain Science, Harvard University, Cambridge MA 02138

[8]Department of Molecular and Cellular Biology, Harvard University, Cambridge MA 02138

Conflict of Interest: The authors declare no competing financial interests.

Correspondence should be addressed to Correspond: schoppik@gmail.com

Cite as: J. Neurosci ; 10.1523/JNEUROSCI.1711-17.2017

Alerts: Sign up at www.jneurosci.org/cgi/alerts to receive customized email alerts when the fully formatted version of this article is published.

Gaze-stabilizing central vestibular neurons project asymmetrically to extraocular motoneuron pools

David Schoppik[1], Isaac H. Bianco[2], David A. Prober[3], Adam D. Douglass[4], Drew N. Robson[5], Jennifer M.B. Li[5], Joel S.F. Greenwood[6], Edward Soucy[7], Florian Engert[7,8], and Alexander F. Schier[7,8]

[1]*Departments of Otolaryngology, Neuroscience & Physiology, and the Neuroscience Institute, New York University School of Medicine, New York, NY 10016* — [2]*Department of Neuroscience, Physiology and Pharmacology, University College London WCE1 6BT England* — [3]*Division of Biology, Caltech, Pasadena CA 91125* — [4]*Department of Neurobiology and Anatomy, University of Utah, Salt Lake City UT 84132* — [5]*Rowland Institute at Harvard, Cambridge MA 02142* — [6]*Department of Neuroscience, Yale University School of Medicine, New Haven CT 06510* — [7]*Center for Brain Science, Harvard University, Cambridge MA 02138* — [8]*Department of Molecular and Cellular Biology, Harvard University, Cambridge MA 02138*

Correspond: schoppik@gmail.com

Abstract

Within reflex circuits, specific anatomical projections allow central neurons to relay sensations to effectors that generate movements. A major challenge is to relate anatomical features of central neural populations — such as asymmetric connectivity — to the computations the populations perform. To address this problem, we mapped the anatomy, modeled the function, and discovered a new behavioral role for a genetically-defined population of central vestibular neurons in rhombomeres 5-7 of larval zebrafish. First, we found that neurons within this central population project preferentially to motoneurons that move the eyes downward. Concordantly, when the entire population of asymmetrically-projecting neurons was stimulated collectively, only downward eye rotations were observed, demonstrating a functional correlate of the anatomical bias. When these neurons are ablated, fish failed to rotate their eyes following either nose-up or nose-down body tilts. This asymmetrically-projecting central population thus participates in both up and downward gaze stabilization. In addition to projecting to motoneurons, central vestibular neurons also receive direct sensory input from peripheral afferents. To infer whether asymmetric projections can facilitate sensory encoding or motor output, we modeled differentially-projecting sets of central vestibular neurons. Whereas motor command strength was independent of projection allocation, asymmetric projections enabled more accurate representation of nose-up stimuli. The model shows how asymmetric connectivity could enhance the representation of imbalance during nose-up postures while preserving gaze-stabilization performance. Finally, we found that central vestibular neurons were necessary for a vital behavior requiring maintenance of a nose-up posture: swim bladder inflation. These observations suggest that asymmetric connectivity in the vestibular system facilitates representation of ethologically-relevant stimuli without compromising reflexive behavior.

Significance Statement

Interneuron populations use specific anatomical projections to transform sensations

43 into reflexive actions. Here we examined how the anatomical composition of a
44 genetically-defined population of balance interneurons in the larval zebrafish relates to
45 the computations it performs. First, we found that the population of interneurons that
46 stabilize gaze preferentially project to motoneurons that move the eyes downward.
47 Next, we discovered through modeling that such projection patterns can enhance the
48 encoding of nose-up sensations without compromising gaze stabilization. Finally we
49 found that loss of these interneurons impairs a vital behavior, swim bladder inflation, that
50 relies on maintaining a nose-up posture. These observations suggest that anatomical
51 specialization permits neural circuits to represent relevant features of the environment
52 without compromising behavior.

53

54 Introduction

55 Neural circuits utilize populations of interneurons to relay sensation to downstream
56 effectors that in turn generate behavior. The anatomical composition of interneuron
57 populations has provided insight into its function. For example, interneuron populations
58 are often organized into maps composed of non-uniformly sized sets of neurons
59 similarly sensitive to particular features (Kaas, 1997). Such visual topography in the
60 thalamus (Connolly and Essen, 1984) and cortex (Daniel and Whitteridge, 1961)
61 magnifies the input from the central visual field. This magnification is thought to underlie
62 enhanced perceptual acuity (Duncan and Boynton, 2003). Preferential anatomical
63 organization is thought to facilitate adaptive olfactory (Hansson and Stensmyr,
64 2011), visual (Barlow, 1981; Xu et al., 2006), somatosensory (Adrian, 1941; Catania
65 and Remple, 2002), and auditory (Bendor and Wang, 2006; Knudsen et al., 1987)
66 computations. However, little is known about how these anatomical asymmetries
67 within populations of sensory interneurons determine the activity of their target motor
68 effectors. Motor anatomy shares a similar uneven organization (Kuypers, 2011), but
69 the complex spatiotemporal encoding of muscle synergies have made comparable
70 dissection of motor circuits more challenging (Harrison and Murphy, 2014; Levine
71 et al., 2012; Shenoy et al., 2013). Even where descending cortical (Lemon, 2008)
72 or brainstem (Esposito et al., 2014) neurons synapse directly on motoneurons, the
73 complexity of most behaviors make it difficult to relate anatomy to function. Data relating
74 the anatomical projections of interneuron populations to their function is needed to
75 address this problem.

76 By virtue of their defined connectivity, interneurons within central reflex circuits offer
77 the opportunity to explore the relationship between population-level anatomical
78 properties and function in a simpler framework. Vestibular interneurons, an ancient and
79 highly conserved population, transform body/head destabilization into commands for
80 compensatory behaviors such as posture and gaze stabilization (Straka and Baker,
81 2013; Straka et al., 2014; Szentágothai, 1964). Gaze-stabilizing vestibular brainstem
82 neurons receive innervation from peripheral balance afferents (Uchino et al., 2001) and
83 use highly stereotyped axonal projections to particular extraocular motoneuron targets
84 that produce directionally-specific eye movements (Iwamoto et al., 1990b; McCrea et
85 al., 1987; Uchino et al., 1982). One anatomical and physiological characterization of
86 up/down-sensitive vestibular neurons in the cat suggested a potential 3:1 bias towards

87 neurons responsible for downward eye movements (Iwamoto et al., 1990a) However,
88 extracellular recording experiments may be subject to selection bias. Further, as
89 selective activation has been impossible, whether there are functional correlates of
90 putative anatomical specialization remains unknown.

91 To study the relationship between the anatomical specializations of interneuron
92 populations and their functions, we investigated a genetically-defined population
93 of vestibular brainstem neurons in a model vertebrate, the larval zebrafish. Larval
94 zebrafish face well-defined challenges that necessitate control of body orientation in
95 the vertical/pitch axis (i.e. nose-up/nose-down). First, larval zebrafish rely on vestibular
96 sensation to guide upward swimming to the water's surface to gulp air and inflate their
97 swim bladders, a vital organ necessary to maintain buoyancy (Goolish and Okutake,
98 1999; Riley and Moorman, 2000). Further, fish actively maintain a nose-up posture
99 (Ehrlich and Schoppik, 2017), permitting them to efficiently maintain their position in
100 the water column despite being slightly denser than their surroundings (Aleyev, 1977;
101 Stewart and McHenry, 2010). Larval zebrafish utilize vestibular brainstem neurons to
102 stabilize gaze by performing torsional and vertical eye movements (Bianco et al., 2012).
103 These same neurons project to nuclei responsible for movement initiation and pitch
104 tilts (Pavlova and Deliagina, 2002; Severi et al., 2014; Thiele et al., 2014; Wang and
105 McLean, 2014).

106 We leveraged known properties of the gaze-stabilization circuit to relate the anatomy of
107 a genetically-defined population of vestibular brainstem neurons and their function. Our
108 study reports three major findings. First, we discovered that central vestibular neurons in
109 rhombomeres 5-7 (r5-r7) project preferentially to extraocular motoneurons that move the
110 eyes down. Ablation of these neurons eliminates counter-rotation of the eyes following
111 body tilts, establishing a role in gaze-stabilization. Second, modeling revealed that
112 asymmetrically projecting neurons could enhance the capacity to represent nose-up
113 stimuli without compromising gaze-stabilization. Third, we discovered that fish do not
114 inflate their swim bladders following ablation of these interneurons. Taken together,
115 our data suggest that the anatomical specialization we observe permits sensory
116 specialization while maintaining reflexive capabilities.

117

Methods

Fish Care

120 All protocols and procedures involving zebrafish were approved by the Harvard
121 University Faculty of Arts & Sciences Standing Committee on the Use of Animals in
122 Research and Teaching (IACUC). All larvae were raised at 28.5° C, on a standard 14/10
123 hour light/dark cycle at a density of no more than 20-50 fish in 25-40mL of buffered
124 E3 (1mM HEPES added). When possible, experiments were done on the mitfa-/-
125 background to remove pigment; alternatively, 0.003% phenylthiourea was added to
126 the medium from 24hpf onwards and changed daily. Larvae were used from 2 days
127 post-fertilization (dpf) to 11 dpf. During this time, zebrafish larvae have not determined
128 their sex.

Behavior

130   Torsional eye movements were measured following step tilts delivered using an
131   apparatus similar in design to (Bianco et al., 2012). All experiments took place in the
132   dark. Larval fish were immobilized completely in 2% low-melting temperature agar
133   (Thermo Fisher 16520), and the left eye was freed. The agar was then pinned (0.1mm
134   stainless minutien pins, FST) to a 5mm^2 piece of Sylgard 184 (Dow Corning) which
135   was itself pinned to Sylgard 184 at the bottom of a 10mm2 optical glass cuvette (Azzota,
136   via Amazon). The cuvette was filled with 1mL of E3 and placed in a custom holder on a
137   5-axis (X,Y,Z,pitch,roll) manipulator (ThorLabs MT3 and GN2). The fish was aligned with
138   the optical axes of two orthogonally placed cameras such that both the left utricle and
139   two eyes were level with the horizon (front camera).

140   The eye-monitoring camera (Guppy Pro 2 F-031, Allied Vision Technologies) used a
141   5x objective (Olympus MPLN, 0.1 NA) and custom image-forming optics to create a
142   100x100 pixel image of the left eye of the fish (6 μm/pixel), acquired at 200Hz. The
143   image was processed on-line by custom pattern matching software to derive an estimate
144   of torsional angle (LabView, National Instruments), and data were analyzed using
145   custom MATLAB scripts (Mathworks, Natick MA). A stepper motor (Oriental Motors
146   AR98MA-N5-3) was used to rotate the platform holding the cameras and fish. The
147   platform velocity and acceleration was measured using integrated circuits (IDG500,
148   Invensense and ADXL335, Analog Devices) mounted together on a breakout board
149   (Sparkfun SEN-09268). Fish were rotated stepwise for 10 cycles: from $0°$ to -60°,
150   where positive values are nose-down, then from -60° to 60°, and then back to $0°$ in 10°
151   increments, with a peak velocity of 35°/sec. The inter-step interval was 5 seconds, and
152   the direction of rotation was then reversed for the next sequence of steps.

153   The eye's response across the experiment was first centered to remove any offset
154   introduced by the pattern-matching algorithm. Data were then interpolated with a cubic
155   spline interpolation to correct for occasional transient slowdowns (i.e. missed frames)
156   introduced by the pattern-matching algorithm. The eye's velocity was estimated by
157   differentiating the position trace; high-frequency noise was minimized using a 4-pole
158   low-pass Butterworth filter (cutoff = 3Hz). Each step response was evaluated manually;
159   trials with rapid deviations in eye position indicative of horizontal saccades or gross
160   failure of the pattern-matching algorithm were excluded from analysis. The response
161   to each step for a given fish was defined as the mean across all responses to that step
162   across cycles. The gain was estimated by measuring the peak eye velocity occurring
163   over the period 375-1000 ms after the start of the step. The steady-state response was
164   estimated by measuring the mean eye position over the final 2 sec of the step; the range
165   was the difference between the most eccentric nose-up and nose-down steady-state
166   angles.

167   Gain was evaluated over the range from +30° to -30°, i.e. the first three steps away
168   from the horizontal meridian. We chose this interval for three reasons: 1) Fish spend
169   the overwhelming majority of their time with a body orientation in this range (Ehrlich and
170   Schoppik, 2017) 2) The responses here were the strongest, allowing us confidence in
171   the dynamic capacity of the system without encountering the biophysical limits imposed
172   by orbital structure 3) Because the utricle conveys information both about static and
173   dynamic changes in orientation, the eyes adopt an increasingly eccentric rotation as the
174   stimulus progresses, potentially constraining dynamic range.

175

Transgenic Lines

177 Tg(-6.7FRhcrtR:gal4VP16):-6.7FRhcrtR was amplified the using a nested PCR
178 strategy. First, a 6775bp DNA fragment immediately upstream of the Fugu rubripes
179 hcrtr2 start site was amplified from genomic DNA, using a high-fidelity polymerase
180 (PfuUltra II Fusion, Stratagene) with primers 5'-AATCCAAATTCCCAGTGACG-3' and
181 5'-CCAGATACTCGGCAAACAAA-3' , 56° C annealing temperature, 1:45 elongation
182 time. The PCR product was TOPO cloned into a TA vector (Thermo Fisher). Using
183 the resulting plasmid as a template, a 6732bp fragment was amplified using primers
184 5'-AATCCAAATTCCCAGTGACG-3' and 5'-CCAGATACTCGGCAAACAAA-3'
185 55° C annealing temperature, 1:45 elongation and similarly TOPO cloned into a
186 GATEWAY-compatible vector (PCR8/GW, Thermo Fisher). The resulting entry
187 vector was recombined into a destination vector upstream of gal4-VP16, between
188 Tol2 integration arms (Urasaki et al., 2006). Tg(UAS-E1b:Kaede)s1999t embryos
189 were injected at the one-cell stage with 0.5nL of 50ng/uL plasmid and 35ng/uL Tol2
190 transposase mRNA in water, and their progeny screened for fluorescence. One founder
191 produced three fluorescent progeny; one survived. To identify transgenic fish without
192 using a UAS reporter, potential carriers were genotyped using the following primers to
193 generate a 592bp product spanning the upstream Tol2 arm and the start of the Fugu
194 sequence: 5'-CAATCCTGCAGTGCTGAAAA-3' and 5'-TGATTCATCGTGGCACAAAT-3'
195 57° C annealing temperature, 0:30 elongation time. The complete expression pattern
196 has been described elsewhere (Lacoste et al., 2015) and is part of the Z-brain atlas
197 (Randlett et al., 2015)

198 Tg(14xUAS-E1b:hChR2(H134R)-EYFP):hChR2(H134R)-EYFP (Zhang et al., 2007) was
199 subcloned downstream of 14 copies of a UAS element and an E1b minimal promoter
200 in a vector containing an SV40 polyA sequence and Tol2 recognition arms (Urasaki
201 et al., 2006). This vector was co-injected with tol2 transposase mRNA into TLAB
202 embryos at the single cell stage. Potential founders were screened by crossing to
203 Tg(isl1:Gal4-VP16,14xUAS:Kaede)(Pan et al., 2011) and monitoring tail movements in
204 response to blue light from an arc lamp on a stereomicroscope (Leica MZ16) at 30hpf.

205 The following transgenic lines were used: Tg(UAS-E1b:Kaede)s1999t (Scott et al.,
206 2007), Tg(isl1:GFP) (Higashijima et al., 2000), Tg(UAS:KillerRed) (Bene et al., 2010),
207 Tg(UAS-E1b:Eco.NfsB-mCherry) (Pisharath et al., 2007), atoh7th241/th241 (Kay et al.,
208 2001); Tg(atoh7:gap43-RFP) (Zolessi et al., 2006), Tg(5xUAS:sypb-GCaMP3) (Nikolaou
209 et al., 2012) and Et(E1b:Gal4-VP16)s1101t (Scott et al., 2007).

210

Anatomy

212 To generate mosaically-labeled fish, 0.5nL of 30ng/μL plasmid DNA
213 (14xUAS-E1b:hChR2(H134R)-EYFP (Douglass et al., 2008) or UAS-Zebrabow (Pan et
214 al., 2013)) was injected in water at the one-cell stage into Tg(-6.7FRhcrtR:gal4VP16);
215 Tg(isl1:GFP) fish. Embryos were screened at 24-48hpf. The majority (80%) of injected
216 fish were excluded due to deformities or developmental arrest. The remaining fish were
217 screened at 72hpf under a fluorescent stereoscope (Leica MZ16) with a high-pass
218 GFP emission filter for YFP fluorescence or a Cy3 emission filter for dTomato. As

219 Tg(-6.7FRhcrtR:gal4VP16) will label the skin and notochord early (36-48hpf) and
220 fluorescence in either structure is relatively easy to visualize, embryos with mosaic
221 labeling (usually 1-10 cells) in these structures were selected. On average, 1-2% of
222 injected embryos were retained for high-resolution screening. Larvae were anesthetized
223 (0.016% w/v tricaine methane sulfonate, Sigma A5040) mounted dorsally at 5-7dpf and
224 imaged on a confocal microscope (Zeiss 510, 710, or 780, using either a 20x 1.0N.A., a
225 40x 1.1 N.A. or a 63x 1.0 N.A. objective with Zen 2010, 8-bit acquisition) with excitation
226 of 488nm (GFP) and 514nm (EYFP), and emission for the two channels was either
227 separated at 550nm by a glass dichroic filters or a tunable filter. The two channels could
228 reliably be separated provided the level of EYFP was strong relative to GFP.

229 Most of the fish selected for confocal imaging had some neurons labeled in the
230 brain, but on average, only 0.5%-2% (i.e. 5-20 for every 1000) of injected embryos
231 would have vestibular nucleus neurons that were both bright and sufficiently isolated
232 enough to trace. Neurons were only included in the study if their axon could be traced
233 unambiguously throughout its entirety to a distinct cell body; qualitatively, the asymmetry
234 persisted among excluded fish. Neurons were traced manually with the assistance
235 of the ImageJ plugin Simple Neurite Tracer (Longair et al., 2011). Cell bodies of the
236 oculomotor and trochlear nuclei were localized manually using the Fiji/ImageJ ROI
237 functionality (Schindelin et al., 2012). Superior oblique motoneurons were found in nIV
238 and superior rectus motoneurons were the most ventral somata in nIII (Greaney et al.,
239 2016). All images were adjusted linearly, using the Brightness & Contrast functionality
240 in Fiji/ImageJ (Schindelin et al., 2012). For display purposes, a non-linear histogram
241 adjustment (gamma = 0.5) was applied to the maximum intensity projection in Figure
242 1b and 2a to increase the relative brightness of thin axonal arbors, and, for Figure 2a, to
243 make clear the sparse nature of the label.

244 Retrograde labeling of the ocular motor nuclei was done as previously described
245 (Greaney et al., 2016; Ma et al., 2010). In brief, crystals of fluorescently-conjugated
246 dextrans (10,000 MW, Thermo Fisher D-1824 or D-22914) were placed in the left orbit
247 of anesthetized 5-7dpf fish. In fish, the superior eye muscles receive projections from
248 the contralateral motor nuclei, making the relevant neurons in nIV (superior oblique)
249 and nIII (superior rectus) easy to discriminate, as they were exclusively labeled on the
250 contralateral (right) side.

251 Focal electroporations were done as detailed previously (Bianco et al., 2012; Tawk
252 et al., 2009). Briefly, anesthetized larvae (2 dpf) were immobilized in low-melting
253 temperature agarose. Micropipettes (tip diameter of 1-2 mm) were filled with a solution
254 containing 1 mg/ml gap43-EGFP plasmid DNA in distilled water. To target the vestibular
255 nucleus neurons, the pipette was placed at the lateral limit of rhombomere 5, using
256 the decussation of the Mauthner axon midline crossing as a landmark. A Grass SD9
257 stimulator (Grass Technologies) was used to deliver three trains of voltage pulses
258 in succession, with 1 s interval between trains. Each train was delivered at 200Hz
259 for 250ms, 2ms on time, with an amplitude of 30V. Larvae were imaged at 5dpf on a
260 custom multi-photon microscope at 790 nm.
261
262 **Lesions**

263 Single-cell ablations were performed using a pulsed infrared laser (SpectraPhysics
264 MaiTai HP) at 820nm (80MHz repetition rate, 80 fs pulse duration) at full power:
265 200mW (2.5nJ) measured at the specimen with a power meter (ThorLabs S130C). Fish
266 were mounted dorsally in 2% low-melt agarose in E3 under a 20x 0.95 NA objective
267 (Olympus) and anesthetized as described above. Cell bodies were targeted for ablation
268 based on anatomical location, starting with the most ventro-lateral neurons in the
269 tangential nucleus and then moving dorso-medially through the tangential and medial
270 vestibular nucleus. Each cell was exposed to the pulsed infrared laser light for a brief
271 period of time (35-50ms) while the resulting fluorescent emissions were measured;
272 usually, there was a brief pulse of light that saturated the detection optics which was
273 used to shutter the laser. 5-10 neurons/plane were targeted bilaterally, resulting in
274 either loss of fluorescence (Tg(UAS-E1b:Kaede)s1999t and Tg(isl1:GFP)) or increased
275 diffuse fluorescence at the cell body (Tg(UAS-ChR2-E134R-EYFP)). Fish were imaged
276 immediately and 24 hours after ablation to confirm the extent of the lesion. 15% of
277 lesioned fish were excluded because they did not survive a full 24hrs after the lesion.
278 Fish were observed under a stereomicroscope in a petri dish post-lesion to ensure
279 the presence of spontaneous horizontal saccades and normal jaw movements; all
280 lesioned fish showed both. Fish for lesions were 4-5 dpf, as preliminary experiments
281 showed that plasma formation was more effective in younger fish, and were selected
282 to be the brightest in the clutch (likely doubly homozygous for UAS-E1b:Kaede and
283 6.7FRhcrtR:gal4VP16).

284 As previously described (Bianco et al., 2012), the eye movements in younger fish are
285 of lower gain, and 3/17 fish were excluded from analysis because their total range
286 was < 10°. Behavior was always measured at least 4 hours and no more than 8 hours
287 after lesions. The decrease in gain was reported as a percentage of pre-lesion gain,
288 defined as the difference between the median pre-lesion gain and median post-lesion
289 gain normalized by the median pre-lesion gain. To activate KillerRed, green light (Zeiss
290 set 43, 545nm/25) from an arc lamp was focused through a 63x 1.0 NA objective
291 stopped down to fill a 200 μm diameter region for 15 minutes. Fish were mounted
292 dorsally and anesthetized as described above. The focal plane was at the level of the
293 decussation of the Mauthner axons, measured under brightfield illumination. Due to
294 equipment replacement the precise power of the arc lamp could not be measured, but
295 20 minutes of exposure under identical conditions was fatal to the fish. Post-lesion
296 behavior was measured at least 4 hours after the light exposure. To induce apoptosis
297 with nitroreductase, fish were placed in E3 with 7.5mM of metrodinazole (Sigma M1547)
298 in 0.2% v/v DMSO and behavior was measured 24hrs later (Curado et al., 2007). The
299 presence of mCherry fluorescence was assayed after behavior to determine genotype.

Optical Activation and Analysis

301 Channelrhodopsin-induced eye movements were monitored using the same apparatus
302 used for measuring tilt-induced behavior, with the addition of a fiber-coupled laser on an
303 independent micromanipulator (Arrenberg et al., 2009; Schoonheim et al., 2010). Fish
304 were immobilized and mounted as before, and agar was removed above the head as
305 well as the left eye. Stimulus was generated by a 100mW 473nm diode laser (Shanghai
306 DreamLasers SDL-473-100MFL) coupled by the manufacturer to a 50 μm inner diameter
307 0.22 NA multimode fiber (ThorLabs AFS50/125Y) that itself was butt-coupled to a 10mm

308 cannula made from the same diameter fiber (ThorLabs AFS50/125YCANNULA). Power
309 at the cannula tip was 30-60mW, measured with a power meter (ThorLabs S130C).
310 The fiber tip was placed above the ear, evenly-centered between the eyes, and 1mm
311 above the skin of the fish. Stimuli ranged in duration from 1 μsec to 100 msec, and were
312 presented every 5 seconds. Eye movements were tracked and processed as before,
313 including manual analysis; only fish with at least 25 analyzable responses to a given
314 stimulus were included in the analysis. The response to a given stimulus was quantified
315 by taking the peak angular rotation reached over the first 2 sec.

316 By microinjecting plasmid DNA at the single-cell stage, we generated embryos as above
317 with somatic expression of ChR2-EYFP in random subsets of vestibular neurons, on
318 a blind background, atoh7th241/atoh7th241 (Kay et al., 2001). As with anatomical
319 experiments, between 5-20 fish for each 1000 injected had acceptable expression. Of
320 these, only 1/4 were homozygous for atoh7th241, and only 1/4 of those expressed the
321 allele necessary to confirm blindness by visualizing the absence of retinal ganglion cell
322 axons Tg(atoh7:gap43-RFP). The large number of alleles required and the low success
323 rate limited the number of fish available to test. Tracing individual axonal projections
324 to quantify the absolute number of VNs labeled in a given fish was not possible except
325 in the most sparsely labeled fish. Further, as expected with somatic expression,
326 ChR2-EYFP levels varied considerably across vestibular neurons. To measure the
327 relationship between expression levels/number of labeled neurons and the magnitude
328 of the evoked eye movement, we quantified EYFP fluorescence. Vestibular neurons are
329 the only neurons with rostral MLF projections labeled in Tg(-6.7FRhcrtR:gal4VP16). As
330 such, the total intensity of the MLF projection for a given fish was measured from the
331 rostral-most point behind nIV, stopping caudally where the projection narrows to the
332 midline (rhombomere 4). A single image that summed the intensity of all slices in the
333 confocal stack that contained the MLF projection was used for our measurements. To
334 correct for differences in acquisition parameters, MLF fluorescence was normalized
335 by a measure of acquisition noise. Noise was estimated by measuring the summed
336 fluorescence of a region between the branches of the MLF, which did not contain any
337 neuropil. A value of one indicates no MLF fluorescence differentiable from background
338 noise, two indicates MLF fluorescence twice that of the background, etc.. Ocular
339 responses to blue light were evaluated and reported as above. Responses were
340 evaluated for significance by comparing the median activity 200 ms after the stimulus
341 to the baseline (200 ms before the stimulus).

Model

343 Our model estimated the collective activity of 80 post-synaptic neurons generated
344 by integrating activity from a set of pre-synaptic neurons. We evaluated two free
345 parameters: the number of pre-synaptic neurons in the set (30, 42, 70, 105, 140, 168,
346 180) and the number of inputs on to a given post-synaptic neuron (2-30). Pre-synaptic
347 activity was generated by translating a rate function, derived from the velocity profile
348 of the steps used in the behavioral experiment, into a Poisson train of activity. Step
349 velocity was scaled to match the reported velocity sensitivity (2 spikes/°/sec) of
350 second-order vestibular neurons (Iwamoto et al., 1990a) to generate a rate function for
351 Poisson spikes. The velocity reached a peak of 35 °/sec and lasted 1sec; the model was
352 run at 1kHz. Poisson trains were subjected to an imposed 2msec refractory period. The

353 spikes were then convolved with a decaying exponential with $\tau = 1.5\text{sec}$ to represent
354 an excitatory post-synaptic potential. A random subset of pre-synaptic neurons were
355 selected from the set and summed together to create an input to a post-synaptic
356 neuron. Post-synaptic activity was determined by thresholding the input, subject to a
357 2msec refractory period. The threshold for the post-synaptic neuron was defined as
358 the minimum of an input of 1.8 or 95% of the cumulative distribution of pre-synaptic
359 input strength. One input spike had a value of 1; after convolution, a threshold of 1.8
360 was reached if at least four spikes were present across all inputs over a 4ms period.
361 Changing the threshold ensured that the post-synaptic response would not saturate as
362 the number of inputs increased; the specific threshold did not change the relationships
363 we observed and is expected from the basic properties of extraocular motoneurons
364 (Torres-Torrelo et al., 2012). We generated 80 distinct spike trains, reflecting the
365 number of motoneurons in a given motoneuron pool (Greaney et al., 2016). The total
366 post-synaptic response was defined as the average activity, evaluated where the rate
367 function was positive. The strength of the relationship between the pre-synaptic rate
368 function and the summed post-synaptic response was defined as the coefficient of
369 determination.

371 **Experimental Design and Statistical Analysis**

372 As data were not normally distributed, expected values are reported as the median,
373 variability as the median absolute deviation (MAD), and non-parametric tests of
374 significance were used. Potential differences between groups (e.g. up tilts vs. down)
375 were evaluated using the Wilcoxon rank sum test, and the Wilcoxon signed rank test
376 was used to test whether a distribution had a median different from zero (e.g. change in
377 performance post-lesion). Significance was determined at $p < 0.05$.

378 # Results

379 ## A genetically-defined population of brainstem neurons projects
380 ## preferentially to extraocular motoneurons that move the eyes
381 ## downward

382 We adopted a molecular approach to characterize a subset of vestibular
383 brainstem neurons in the larval zebrafish. We used a transgenic line of zebrafish,
384 Tg(-6.7FRhcrtR:gal4VP16) that drives expression of a transcription factor (Gal4) in a
385 restricted subset of neurons, including those in r5-r7 (Lacoste et al., 2015; Randlett et
386 al., 2015). When crossed with other transgenic lines that contain an upstream activating
387 sequence (UAS), Gal4 induces selective expression of particular genes useful for
388 visualization, and for chemical or light-mediated manipulation. We first crossed the
389 Tg(-6.7FRhcrtR:gal4VP16) to the Tg(UAS-E1b:Kaede)s1999t line to selectively drive a
390 red fluorescent protein. In addition, we performed these experiments on a transgenic
391 background, Tg(isl1:GFP), that constitutively labeled cranial motoneurons, including
392 extraocular motoneurons, with a green fluorescent protein.

393 Within r5-r7 (delineated by the rostro-caudal extent of the facial nucleus, Figure 1B),
394 we observed expression in ~200 neurons that, in aggregate, comprise a subset of
395 two bilateral vestibular nuclei. The first was the previously characterized utricle signal

9

396 recipient tangential nucleus (Bianco et al., 2012), located adjacent to the ear. The
397 second was the medial vestibular nucleus (Highstein and Holstein, 2006) separated
398 from the tangential nucleus by the lateral longitudinal fasciculus. Figure 1A-1C show the
399 gross morphology of these neurons and their axonal projections to the extraocular motor
400 nuclei. In aggregate, we observed that the axon bundle from these vestibular neurons
401 crosses the midline, ascends rostrally along the medial longitudinal fasciculus (MLF),
402 and projects to extraocular motor nuclei nIII and nIV (Figure 1D-1F).

403 The utricular vestibulo-ocular reflex utilizes two independent "channels," or defined
404 neural pathways from peripheral sensation to motor output, to stabilize gaze following
405 pitch and roll tilts. At the level of the extraocular motoneurons, in the larval zebrafish
406 the two channels are segregated along the dorso-ventral axis. First, the ventral-most
407 extraocular motoneurons in nIII project to the inferior oblique (IO) and superior rectus
408 (SR) motoneurons. Together, IO/SR move the eyes up following nose-down pitch tilts.
409 Second, the dorsal-most extraocular motoneurons in nIII project to the inferior rectus
410 (IR), and the dorsally-located nucleus nIV projects exclusively to the superior oblique
411 (SO). Together, IR/SO move the eyes down following nose-up pitch tilts. The somatic
412 organization of nIII and nIV is stable after 5 days post-fertilization (Greaney et al., 2016).
413 Finally, previous electromyographic recordings demonstrates that the SR (nIII) and SO
414 (nIV) muscles are exclusively active during either the nose-down or nose-up phase of
415 pitch-tilts supporting the independence of the two channels (Favilla et al., 1983).

416 Complementarily, pitch-sensitive vestibular nucleus neurons split into two subtypes,
417 each projecting to only one pair of extraocular motoneurons (Uchino et al., 1982). The
418 first group arborizes exclusively in nIII, innervating IO/SR. The second arborizes in both
419 nIII and nIV, innervating SO/IR. Since nIV is comprised only of extraocular motoneurons
420 that innervate SO, a collateral projection to nIV differentiates vestibular interneurons that
421 respond to nose-up pitch tilts from those that respond to nose-down.

422 To determine if vestibular neurons labeled in Tg(-6.7FRhcrtR:gal4VP16) comprise
423 both nose-up and nose-down subtypes, we examined their collective projections. We
424 observed that their projection terminated near the ventral-most extraocular motoneurons
425 in nIII (wide view in Figure 1G, close up Figure 1H-1I). The second prominent projection
426 from vestibular neurons goes to extraocular motoneurons in nIV (wide view in Figure
427 1J, close-up Figure 1K-1L). We conclude that the vestibular neurons labeled in r5-r7 in
428 Tg(-6.7FRhcrtR:gal4VP16) are poised to respond during both nose-up and nose-down
429 pitch tilts.

430 To test whether the vestibular neurons labeled in Tg(-6.7FRhcrtR:gal4VP16) projected
431 symmetrically to extraocular motoneurons, we examined the axon collaterals of
432 singly-labeled neurons. To differentiate nose-up from nose-down vestibular neurons,
433 we manually traced the axons of vestibular neurons and used the labeled cranial
434 motor nuclei to categorize their projections, based on the presence/absence of a
435 collateral projection to nIV. We labeled stochastic subsets of vestibular neurons
436 by injecting a plasmid encoding a fluorescent protein into one-cell embryos,
437 Tg(-6.7FRhcrtR:gal4VP16). Experiments were performed on the Tg(isl1:GFP)
438 background to co-label extraocular motoneurons. The majority of labeled neurons
439 (25/27) had only an ascending collateral; the remaining two had a bifurcated axon
440 that both ascended and descended along the MLF. We found that the overwhelming

441 majority (23/27) of labeled vestibular neuron axons had a dorsal collateral projecting
442 to nIV (i.e. nose-up/eyes-down vestibular neurons). One example neuron from the
443 majority population is shown projecting to nIV in Figure 2A-2D and reconstructed as a
444 schematic in Movie M1. In contrast, one example neuron from the minority population,
445 projecting exclusively to nIII with a collateral to the superior rectus motoneurons, is
446 shown in Figure 2E-2G, and reconstructed in Movie M2. Somata of neurons projecting
447 exclusively to nIII were intermingled with those with projections to nIV. By examining
448 labeled neurons at two time points (5 and 11 days post-fertilization) we found that the
449 characteristic collateral projection to nIV in traced vestibular neurons remained unaltered
450 (Figure 3).

451 Our genetically-based labeling technique is limited to neurons within the population
452 labeled in Tg(-6.7FRhcrtR:gal4VP16). To complement our initial characterization with
453 an unbiased sample of vestibular neurons in r5-r7, we examined the projections of
454 vestibular neurons that had been electroporated with a membrane-targeted fluorescent
455 protein in wild-type animals. Of 20 electroporated animals with singly-labeled neurons in
456 the vestibular nuclei, 15 neurons had an ascending branch along the medial longitudinal
457 fasciculus. 12 of these (80%) had a prominent projection to nIV. Taken together, our
458 data support the conclusion that vestibular neurons in the larval zebrafish project
459 preferentially to extraocular motoneurons that move the eyes down.

460 To determine whether there was anatomical evidence that the axonal collaterals
461 contained synapses, we labeled presynaptic puncta in Tg(-6.7FRhcrtR:gal4VP16)
462 by crossing to Tg(5xUAS:sypb-GCaMP3) to selectively express a fluorescent protein
463 fused to the presynaptic protein synaptophysin (Nikolaou et al., 2012). We then labeled
464 the extraocular motoneurons by retro-orbital dye fill. We confirmed the presence of
465 presynpatic puncta proximal to the soma and dendrites of SO and SR motoneurons
466 (Figure 4). Recent expansion microscopy work together with anti-synaptotagmin2b
467 staining confirmed the presence of synaptic puncta between vestibular neurons labeled
468 in Tg(-6.7FRhcrtR:gal4VP16) and extraocular motoneuron somata and dendrites (L.
469 Freifeld and E. Boyden, unpublished observations). These results suggest that the axon
470 collaterals from vestibular neurons labeled in Tg(-6.7FRhcrtR:gal4VP16) likely contain
471 functional synapses.

472

473 **Labeled vestibular neurons are collectively necessary for gaze**
474 **stabilization following both nose-up and nose-down body rotations**

475 To determine whether the transgenically-labeled vestibular neurons constitute a
476 complete set necessary for both upwards and downwards eye movements following
477 body tilts, we measured gaze stabilization (the vestibulo-ocular reflex) before
478 and after their removal. We ablated single vestibular neurons individually with a
479 pulsed infrared laser in Tg(-6.7FRhcrtR:gal4VP16). These fish had been crossed to
480 Tg(UAS-E1b:Kaede)s1999t to express a fluorescent protein in vestibular neurons.
481 Further, experiments were performed on the Tg(isl1:GFP) background that labeled
482 adjacent motoneurons in nVII for control ablations (Figure 5A). Following ablation,
483 qualitative observation revealed that horizontal eye saccades and spontaneous
484 jaw movements were present as in normal fish. Ablations eliminated nearly the

11

485 entire response to body tilts (both nose-up and nose-down): the median decrease
486 in vestibulo-ocular reflex gain was 94.5% ± 3.5% (n = 14, p = $1.2 * 10^{-4}$ Figure 5B).
487 We saw no difference (p = 0.77) in the post-lesion gain for nose-up (0.0165 ± 0.0135)
488 and nose-down (0.02 ± 0.0135) body rotations. In contrast, control lesions of somata
489 in the adjacent facial nucleus (nVII) produced no systematic change in the gain (n

490 = 5, 38.5% ± 24.5%, p = 0.41) or the range (31% ± 52%, p = 0.44, Figure 5C) of the

491 vestibulo-ocular reflex.

492 To confirm the finding that the labeled neurons in Tg(-6.7FRhcrtR:gal4VP16) were
493 necessary for the normal vestibulo-ocular reflex following pitch tilts, we used two
494 additional ablation techniques to target neurons labeled in Tg(-6.7FRhcrtR:gal4VP16).
495 First, by crossing to Tg(UAS-E1b:Eco.NfsB-mCherry) we selectively expressed a
496 protein, nitroreductase (nfsb) that caused neurons to die on exposure to a prodrug,
497 metronidazole (Curado et al., 2007; Pisharath et al., 2007). After exposure to
498 metronidazole, the vestibulo-ocular reflex was significantly impaired in larvae that
499 expressed nfsb compared to their siblings that did not (n=5, p = 0.008, Figure 5C). Next,
500 we crossed Tg(-6.7FRhcrtR:gal4VP16) to Tg(UAS-KillerRed) to selectively express
501 a protein, Killer Red, that causes neurons to die on exposure to green light (Bene et
502 al., 2010). After exposing the hindbrain to green light, the vestibulo-ocular reflex was
503 significantly impaired in larvae that expressed Killer Red compared to similarly exposed
504 siblings (n=5, p = 0.008, Figure 5C). We conclude that vestibular neurons labeled in
505 Tg(-6.7FRhcrtR:gal4VP16) are necessary for compensatory eye movements following
506 either nose-up or nose-down body pitch tilts.

507 **Labeled vestibular neurons, collectively activated, rotate the eyes**
508 **down**

509 The circuit that enables correct gaze stabilization following pitch and roll body tilts
510 (Figure 6) permits a specific prediction about the eye movements that might follow
511 collective activation. Three key features of this circuit enable this prediction: 1. two
512 distinct channels selectively sensitive to nose-up and nose-down rotations, 2. excitatory
513 central neurons that all cross the midline, and 3. superior extraocular motoneurons
514 that cross back. Figure 6C-6D show the torsional response to nose-up and nose-down
515 body tilts. There, utricular hair cells in both the left and right ear sense the same pitch
516 tilts. The projection patterns ensure that inputs from a given ear contacts the correct
517 superior eye muscle on the ipsilateral side, and the correct inferior eye muscle on
518 the contralateral side. In contrast, when the fish rolls, both nose-up and nose-down
519 channels ipsilateral to the roll are activated. The two superior muscles are then
520 activated ipsilaterally, while the two inferior muscles are activated contralaterally. In
521 this way, a single circuit can respond appropriately to the two cardinal directions of body
522 rotation sensed by the utricle, the sole source of vestibular sensation in young zebrafish
523 (Beck et al., 2004; Bianco et al., 2012; Mo et al., 2010; Roberts et al., 2017).

524 Collectively activating all utricle signal recipient vestibular neurons is therefore
525 equivalent to the fish rolling both leftward and rightward simultaneously.
526 Consequentially, all four eye muscles on both sides would be expected to contract
527 together. If no eye movement were to result, we would conclude that despite the
528 anatomical asymmetry, the nose-up and nose-down vestibular neuron pools were
529 functionally equivalent. In contrast, a net downward rotation reflects stronger
530 activation of the SO/IR motoneurons (nose-up, Figure 6C) and weaker activation of

531   the SR/IO motoneurons (nose-down, Figure 6D). A net upward rotation reflects
532   the opposite. Any vertical component (SO/SR vs IO/IR) to the eye movement would
533   reflect uneven activation of neurons in the left vs. right hemisphere (Figure 6B),
534   and would be dissociable from the torsional component. We hypothesized that the
535   gaze-stabilization circuit predicts that any systematic eye movement observed along the
536   nose-up/nose-down axis following collective activation of vestibular brainstem neurons
537   must reflect a functional bias in the set of activated neurons.

538   To determine whether the asymmetry among the population of neurons we observed
539   is functional, we measured eye rotations following collective activation of brainstem
540   neurons labeled in Tg(-6.7FRhcrtR:gal4VP16). We expressed the light-sensitive cation
541   channel, channelrhodopsin-2 (ChR2) and used a fiber-optic cannula (Arrenberg et al.,
542   2009) to target blue light to labeled vestibular neurons in Tg(-6.7FRhcrtR:gal4VP16);
543   Tg(UAS:ChR2(H134R)-EYFP) fish. Since blue light evoked eye movements in
544   wild-type fish (Movie M3), we performed all activation experiments using a blind mutant
545   lacking retinal ganglion cells: atoh7$^{th241/th241}$; Tg(atoh7:gap43-RFP) (Kay et al., 2001).
546   Strikingly, in every transgenic fish tested, the eyes rotated downward in response to
547   blue light flashes, as if the nose of the fish had moved up. We observed no systematic
548   vertical component to the eye's rotation. Across fish (n = 10) the amplitude of eye
549   rotation (Figure 7a, black line) scaled with the duration of the light flash, with a peak

550   response of 45°/sec. Crucially, control siblings (n = 3) not expressing ChR2 did not
551   respond to light flashes (Figure 7A, gray line). Laser-mediated ablation of vestibular
552   neurons abolished the light-evoked eye rotation (n=10, Figure 7B). Activation of the
553   population of vestibular neurons is therefore sufficient to rotate the eyes downward,
554   consistent with the asymmetric distribution of anatomical projections.

555   We extended our test of sufficiency by activating all of the neurons in the region of the
556   vestibular nucleus using a line reported (Scott et al., 2007) to drive expression in all
557   neurons, Et(E1b:Gal4-VP16)s1101t. In all fish tested (n=6), we evoked downward eye
558   rotations in the torsional plane corresponding to nose-up tilts (Figure 7C, Movie M4, note
559   the corruptive horizontal component present in one trace). Both genetically restricted
560   and unbiased activation of vestibular neurons produced net downward eye rotations,
561   and thus the gaze-stabilizing population of vestibular neurons is functionally asymmetric.

562   To test whether selective activation of vestibular neurons is sufficient to rotate the eyes,
563   and to estimate the variability across neurons, we expressed ChR2 stochastically
564   in subsets of neurons in Tg(-6.7FRhcrtR:gal4VP16) fish on a blind background
565   (atoh7th241/th241; Tg(atoh7:gap43-RFP). Of 27 sparsely labeled fish, 12 had
566   expression in vestibular neurons. As expected from the uneven anatomy, all 12 had
567   neurons with axon collaterals to nIV. Consistent with our categorization of nIV-projecting
568   neurons as "nose-up/eyes-down" we could evoke significant downward eye movements
569   in 10/12 fish (0.23° ± 0.16°, p < 0.05 relative to baseline for each fish, Figure 7D). Across
570   all fish, the intensity of the projection in the MLF, an estimate of ChR2 expression,
571   predicted the magnitude of the evoked response (Spearman's rank correlation
572   coefficient = 0.45, p = 0.02, n = 27). These results reveal that subsets of nIV-projecting
573   vestibular neurons are sufficient, but vary in their ability to generate downward eye
574   rotations.
575

A simple model shows how biased vestibular populations can better represent nose-up sensations without compromising motor performance

Our data support the hypothesis that labeled premotor vestibular neurons are asymmetrically distributed, over-representing nose-up body tilts, and capable of producing downward eye rotations. To infer whether such an asymmetry might impact motor output and/or sensory encoding, we built a simple model of the synapse between vestibular and extraocular motoneurons. We simulated the ability of differently-sized populations to relay a step in body tilt (encoded by vestibular neuron activity) across a single synapse to produce an eye movement command (encoded by extraocular motoneuron activity). We constrained model parameters and assumptions to reflect known anatomical and electrophysiological properties (Methods). For this model, we assume that the activity of the vestibular neurons is a function of body tilt. We systematically varied two free parameters: the size of the vestibular population, and the number of vestibular neurons that contact a single extraocular motoneuron. As nose-up and nose-down neurons function during distinct phases of pitch tilts (Figure 6) we simulated a single generic population. We evaluated two features of simulated motoneuron activity. First, as a measure of output strength, we report the average activity (reflecting the strength of ocular muscular contraction). Next, as a measure of encoding fidelity, we report the correlation between vestibular input and motoneuron output.

We observed that the magnitude of motoneuron activity could be independent of the number of vestibular neurons upstream (vertical axis in Figure 8C). This dissociation derives from the fact that vestibular neurons encoding nose-up and nose-down body rotations converge on to distinct pools of motoneurons. Consequentially, the key variable that determines the magnitude of motoneuron activity is the number of inputs per motoneuron, not the size of the vestibular population from which it is derived. As expected, increasing the number of vestibular inputs onto a single motoneuron increased its firing rate asymptotically (horizontal axis in Figure 8C). We conclude that when downstream effectors are distinct, as for eye movements, a larger pool of premotor neurons does not necessarily predict differences in the magnitude of motoneuron output. For our system, an asymmetric vestibular circuit could maintain comparable behavioral responses along the eyes-up/eyes-down axis.

In contrast, we observed that the size of the vestibular neuron pool could impact the ability of motoneurons to represent the dynamics of a step in body position. Temporal structure emerges in the activity patterns of post-synaptic neurons derived from small population sizes (Figure 8b). This similarity across motoneuron activity patterns reflected the coincidence of a limited set of inputs sufficient for a motoneuron spike at a particular time. To test if this limitation constrains the ability of motoneurons to represent the input function, we measured the variance in the input rate function explained by the summed motoneuron activity (R^2). Larger populations were indeed better than smaller populations, and performance varied with the precise number of pre-synaptic inputs (Figure 8D). Adding a basal level of activity equal to 15% of the peak response

14

621 decreased R^2 but did not change the finding that larger populations were better at
622 representing the input function. We infer from our model that the anatomical asymmetry
623 we observe could permit better encoding of nose-up sensations without compromising
624 gaze-stabilization. If sensory statistics were similarly biased, asymmetric projections
625 from vestibular neurons might therefore be adaptive.

626

627 Premotor vestibular neurons are necessary for a vital and
628 asymmetric postural behavior

629 To maintain buoyancy, larval zebrafish, whose gills do not yet function (Rombough,
630 2007), must swim to and maintain a nose-up posture at the water's surface, where they
631 gulp air, inflating their swim bladder (Goolish and Okutake, 1999). Vestibular sensation
632 is necessary: larval zebrafish without functional utricles fail to inflate their swim bladder
633 and die (Riley and Moorman, 2000). In contrast, vision is not required for this behavior,
634 as blind fish develop normal swim bladders. Gaze-stabilizing vestibular neurons send
635 a second projection to a spinal premotor nucleus, the nucleus of the MLF (nucMLF)
636 (Figure 1), indicating a potential postural role (Bianco et al., 2012).

637 To test if vestibular neurons are necessary for swim-bladder inflation, we focally
638 ablated vestibular neurons at 72hpf, before fish had inflated their swim bladder, in
639 Tg(-6.7FRhcrtR:gal4VP16);Tg(14xUAS-E1b:hChR2(H134R)-EYFP) fish. We evaluated
640 the fish at 144hpf (Figure 9). Only 1/9 lesioned fish (example in Movie M6) had an
641 inflated swim bladder, compared with 40/42 control siblings (example in Movie M7).
642 To confirm these results, we chemogenetically ablated vestibular neurons at 72 hpf
643 in Tg(-6.7FRhcrtR:gal4VP16);Tg(UAS-E1b:Eco.NfsB-mCherry) fish. As with the
644 targeted lesions, only 1/36 double-transgenic fish inflated their swim bladder and
645 survived, while 36/36 of their non-expressing siblings did. We note that in contrast,
646 fish with post-inflation loss of vestibular neurons (e.g. Figure 5) maintain normal
647 swim bladders. These results define a novel role for vestibular neurons labeled in
648 Tg(-6.7FRhcrtR:gal4VP16) in swim-bladder inflation.

649

650 Discussion

651 We investigated how the anatomical composition of a genetically-defined population
652 of vestibular interneurons in the larval zebrafish could constrain its function. We first
653 discovered that genetically-labeled neurons project preferentially to motoneurons that
654 move the eyes downward. Ablation of these neurons eliminated the eye movements
655 normally observed following nose-up/nose-down body tilts, establishing their necessity
656 for gaze stabilization. Next, we found that activation produced downward eye rotations,
657 establishing a functional correlate of the anatomical asymmetry. We modeled similar
658 populations with asymmetric projections, and inferred that such architecture could
659 permit better representation of nose-up stimuli while maintaining gaze stabilization
660 performance. Finally, we discovered that early ablation of these neurons impaired swim
661 bladder inflation, a vital postural task requiring nose-up stabilization. Taken together,
662 we propose that preferential allocation of vestibular resources may improve sensory
663 encoding, potentially enabling larval zebrafish to meet ethologically-relevant challenges

15

664   without compromising behavior.

665   Our study used a transgenic line, Tg(-6.7FRhcrtR:gal4VP16) to reliably access a
666   genetically defined set of neurons in rhombomeres 5-7 in the medial and tangential
667   vestibular nuclei. The rhombomeric and medio-lateral location of these neurons is
668   consistent with the neurons that receive utricular input in the adult frog (Straka, 2003)
669   and chick (Popratiloff and Peusner, 2007) and comprises a subset of neurons that
670   project to extraocular motoneurons in the larval frog (Straka et al., 2001), juvenile
671   zebrafish/goldfish (Suwa et al., 1996) and chick (Gottesman-Davis and Peusner,
672   2010). Tg(-6.7FRhcrtR:gal4VP16) does not label neurons within the superior vestibular
673   nucleus in the rostral hindbrain (Cambronero and Puelles, 2000). This absence is
674   notable in light of our ablation experiments that implicate only the neurons labeled
675   in Tg(-6.7FRhcrtR:gal4VP16) as necessary for the torsional vestibulo-ocular reflex.
676   Neurons in the superior vestibular nucleus receive input predominantly from the anterior
677   canal and the lagena (Straka, 2003), and from the anterior canal in monkeys (Yamamoto
678   et al., 1978). Larval zebrafish do not have functional semicircular canals (Beck et al.,
679   2004) nor has the lagena developed (Bever and Fekete, 2002) at the ages we studied
680   here. Therefore, superior vestibular nucleus neurons would not be expected to respond
681   to body rotations, consistent with our observation that the eyes no longer counter-rotate
682   after lesions of Tg(-6.7FRhcrtR:gal4VP16) positive neurons. Further, the superior
683   vestibular nucleus contains predominantly ipsilaterally-projecting, likely inhibitory inputs
684   in adult rays (Puzdrowski and Leonard, 1994), goldfish (Torres et al., 2008, 1992), frog
685   (Montgomery, 1988), rabbit (Wentzel et al., 1995), cat (Carpenter and Cowie, 1985) and
686   monkey (Steiger and Büttner-Ennever, 1979). In the adult goldfish, such inhibitory inputs
687   to extraocular motoneurons were found to be less effective relative to their excitatory
688   counterparts. If the vestibular circuit were similarly constrained in larval zebrafish, it
689   could explain the smaller downward eye movement we saw after collective activation
690   of all neurons. There, the normal downward eye rotation would be compromised,
691   though not eliminated, by inhibition derived from superior vestibular nucleus neurons not
692   labeled in Tg(-6.7FRhcrtR:gal4VP16) but activated in a pan-neuronal line. We therefore
693   propose that the inputs and output of superior vestibular nucleus neurons not labeled
694   in Tg(-6.7FRhcrtR:gal4VP16) render them unlikely to play a major role in the larval
695   zebrafish torsional vestibulo-ocular reflex.

696   Previous work in larval zebrafish identified the tangential nucleus as the locus of
697   neurons responsible for the utricle-dependent torsional vestibulo-ocular reflex (Bianco et
698   al., 2012). Here, we show similarly profound impairment of the torsional vestibulo-ocular
699   reflex after targeted ablation of a subset of vestibular interneurons in the tangential
700   and medial vestibular nuclei that are labeled in Tg(-6.7FRhcrtR:gal4VP16) larvae.
701   Therefore, we propose that the set of tangential nucleus neurons labeled in labeled
702   in Tg(-6.7FRhcrtR:gal4VP16) are responsible for the utricle signal mediated torsional
703   vestibulo-ocular reflex, as those were ablated both here and in Bianco et al. (2012).
704   Similarly, previous single-cell fills of tangential nucleus neurons revealed three classes
705   of projection neurons: those projecting to the contralateral tangential nucleus, those with
706   a single ascending collateral to nIII/nIV and the nucleus of the MLF and those with both
707   an ascending and descending branch. Ascending and ascending/descending neurons
708   were represented roughly equally (7/16 and 6/16) in the tangential nucleus (Bianco et

16

709 al., 2012). However, we found that the labeled neurons in Tg(-6.7FRhcrtR:gal4VP16)
710 were almost exclusively of the ascending type (25/27). We therefore propose a further
711 refinement: the neurons responsible for the utricle-mediated torsional vestibulo-ocular
712 reflex are likely the subpopulation of ascending neurons within the tangential nucleus
713 labeled in Tg(-6.7FRhcrtR:gal4VP16). This proposal is consistent with anatomical and
714 functional work in juvenile and adult goldfish, where tangential nucleus neurons with
715 ascending processes were shown to respond to nose-up/nose-down tilts (Suwa et al.,
716 1999) Taken together, our molecular approach permits strong hypotheses that define the
717 essential subset of vestibular neurons responsible for a particular behavior.

718 The muscles that generate torsional eye movements in fish are responsible for vertical
719 eye movements in frontal-eyed animals (Simpson and Graf, 1981). The behavioral
720 literature is unclear with respect to whether nose-up/nose down gaze-stabilization is
721 asymmetric. Cats may produce stronger downward eye rotations (Darlot et al., 1981;
722 Maruyama et al., 2004; Tomko et al., 1988), but the literature is conflicted as to whether
723 or not such an asymmetry exists in primates: downward (Baloh et al., 1983; Benson
724 and Guedry, 1971; Matsuo and Cohen, 1984) or no biases (Baloh et al., 1986; Demer,
725 1992; Marti et al., 2006) have both been reported. In foveate vertebrates, the vestibular
726 brainstem contains the final premotor nuclei for smooth pursuit eye movements. Despite
727 similar abilities to perceive both directions of vertical motion (Churchland et al., 2003),
728 both juvenile and mature monkeys (Akao et al., 2007; Grasse and Lisberger, 1992)
729 and humans (Ke et al., 2013) show a stronger downward response. Our model points
730 a way forward: while common laboratory stimuli may elicit largely similar vertical eye
731 movements, an asymmetric population should better encode dynamic variability, such
732 as experienced in natural settings (Carriot et al., 2014). We propose that characterizing
733 the variation in response to more complex body rotations and target tracking paradigms
734 could uncover behavioral signatures of an anatomically biased circuit.

735 We found that larval zebrafish do not inflate their swim bladders after early but not
736 late ablation of vestibular neurons. As autonomic neurons are thought to determine
737 swim bladder volume (Smith and Croll, 2011), we propose that the failure to inflate
738 the swim bladder is secondary to postural impairments that follow loss of vestibular
739 neurons labeled in Tg(-6.7FRhcrtR:gal4VP16). In addition to extraocular motor nuclei,
740 these neurons project to the nucleus of the medial longitudinal fasciculus (nMLF)
741 (Bianco et al., 2012). Recent work has established the necessity and sufficiency
742 of spinal-projecting neurons in the larval zebrafish nMLF for postural control and
743 swim initiation (Severi et al., 2014; Thiele et al., 2014; Wang and McLean, 2014).
744 By virtue of their direct projections, and their necessity for swim bladder inflation, we
745 propose that neurons labeled in Tg(-6.7FRhcrtR:gal4VP16) may affect posture by
746 modulating activity of neurons in the nMLF. As such, our work thus establishes a new
747 molecularly-accessible avenue to explore neural mechanisms underlying postural
748 stabilization.

749 Zebrafish engage in postural behaviors across their lifespan that are well-suited to
750 nose-up sensory specialization. First, as larvae, they swim along a trajectory dictated
751 by the long axis of their body (Aleyev, 1977). Their bodies are denser than water
752 (Stewart and McHenry, 2010), which ought cause them to sink. Instead, they adopt a
753 nose-up bias to their posture (Ehrlich and Schoppik, 2017), which introduces a vertical

754 component to their swims, enabling them to maintain elevation. Second, larval zebrafish
755 must swim to the surface to gulp air necessary to inflate their swim bladder (Goolish
756 and Okutake, 1999). Finally, most adult teleosts engage in aquatic surface respiration
757 throughout life (Kramer and McClure, 1982), a response to low oxygen saturation that
758 necessitates a continuous nose-up posture at the water's surface. Our model shows
759 how the anatomical makeup of the vestibular circuits could better encode the nose-up
760 bias in the statistics of behavior. Our findings thus provide a premotor complement to
761 the "efficient coding" framework used to relate the makeup of sensory systems to the
762 statistics of the environment (Simoncelli, 2003).

763 Asymmetrically organized populations of interneurons are common throughout nervous
764 systems. Asymmetric organization within sensory areas is thought to reflect afferent
765 adaptations (Adrian, 1941; Barlow, 1981; Bendor and Wang, 2006; Catania and
766 Remple, 2002; Hansson and Stensmyr, 2011; Knudsen et al., 1987; Simoncelli, 2003;
767 Xu et al., 2006) but the complexity of most neural circuits makes it challenging to link
768 encoding capacity to adaptive behavior. For asymmetric motor populations, links to
769 behavior are more direct (Esposito et al., 2014; Lemon, 2008; Pasqualetti et al., 2007;
770 Rathelot and Strick, 2009) but the natural sensations that drive these areas are often
771 difficult to define. Our study of vestibular interneurons that play both sensory and
772 premotor roles illustrates how the asymmetric anatomy could better encode nose-up
773 sensations, while maintaining the ability to stabilize gaze. As asymmetric populations
774 of interneurons are common, we propose that other circuits may use similar strategies to
775 meet ethological demands without compromising motor control.

776

Author Contributions

778 Author contributions: DS conceived the study in discussions with IHB, FE and AFS.
779 DS generated the Tg(-6.7FRhcrtR:gal4VP16) line, designed and built the behavioral
780 apparatus/software, collected, analyzed and modeled data and discussed them with
781 IHB, FE and AFS. IHB performed the focal electroporation and imaging used in Figure
782 1a. DP and ADD generated the 14xUAS-E1b:hChR2(H134R)-EYFP construct and
783 line. JG and ES helped design, prototype, assemble, troubleshoot and optimize all
784 hardware. DR and JL designed, built, and maintained the 2-photon microscope and
785 control software; DS and DR developed and optimized the lesion protocol. JL and DR
786 made the gal4-VP16 destination vector. DS and AFS wrote the paper.

787

Acknowledgements

18

Author Information

Author Information: All raw data, analysis, and figure generation code can be downloaded at http://www.schoppiklab.com/ . The authors declare no competing financial interests. Correspondence and requests for reagents or fish lines should be addressed to schoppik@gmail.com , schier@fas.harvard.edu or florian@mcb.harvard.edu .

Bibliography

Adrian ED (1941)   Afferent discharges to the cerebral cortex from peripheral sense organs. *The Journal of Physiology* 100:159–191.

Akao T, Kumakura Y, Kurkin S, Fukushima J, Fukushima K (2007)   Directional asymmetry in vertical smooth-pursuit and cancellation of the vertical vestibulo-ocular reflex in juvenile monkeys. *Experimental Brain Research* 182:469–478.

Aleyev YG (1977) *Nekton* Dr. W. Junk.

Arrenberg AB, Bene FD, Baier H (2009)   Optical control of zebrafish behavior with halorhodopsin. *Proceedings of the National Academy of Sciences* 106:17968–17973.

Baloh RW, Honrubia V, Yee RD, Jacobson K (1986) Vertical visual-vestibular interaction in normal human subjects. *Experimental Brain Research* 64:400–406.

Baloh RW, Richman L, Yee RD, Honrubia V (1983)   The dynamics of vertical eye movements in normal human subjects. *Aviation, Space, and Environmental Medicine* .

Barlow HB (1981)   The Ferrier lecture, 1980: Critical limiting factors in the design of the eye and visual cortex.   *Proceedings of the Royal Society B: Biological Sciences* 212:1–34.

Beck JC, Gilland E, Tank DW, Baker R (2004) Quantifying the ontogeny of optokinetic and vestibuloocular behaviors in zebrafish, medaka, and goldfish.   *Journal of Neurophysiology* 92:3546–3561.

Bendor D, Wang X (2006)   Cortical representations of pitch in monkeys and humans. *Current Opinion in Neurobiology* 16:391–399.

Bene FD, Wyart C, Robles E, Tran A, Looger L, Scott EK, Isacoff EY, Baier H (2010)   Filtering of visual information in the tectum by an identified neural circuit. *Science* 330:669–673.

Benson AJ, Guedry FE (1971) Comparison of tracking-task performance and nystagmus during sinusoidal oscillation in yaw and pitch. *Aerospace Medicine* .

Bever MM, Fekete DM (2002)   Atlas of the developing inner ear in zebrafish. *Developmental Dynamics* 223:536–543.

Bianco IH, Ma LH, Schoppik D, Robson DN, Orger MB, Beck JC, Li JM, Schier

842   AF, Engert F, Baker R (2012)   The tangential nucleus controls a gravito-inertial
843   vestibulo-ocular reflex. *Current Biology* 22:1285–1295.
844   Cambronero F, Puelles L (2000)   Rostrocaudal nuclear relationships in the avian
845   medulla oblongata: A fate map with quail chick chimeras. *The Journal of Comparative*
846   *Neurology* 427:522–545.
847   Carpenter MB, Cowie RJ (1985) Connections and oculomotor projections of the
848   superior vestibular nucleus and cell group 'y'. *Brain Research* 336:265–287.
849   Carriot J, Jamali M, Chacron MJ, Cullen KE (2014)   Statistics of the vestibular input
850   experienced during natural self-motion: Implications for neural processing. *Journal*
851   *of Neuroscience* 34:8347–8357.
852   Catania KC, Remple MS (2002) Somatosensory cortex dominated by the representation
853   of teeth in the naked mole-rat brain.   *Proceedings of the National Academy of*
854   *Sciences* 99:5692–5697.
855   Churchland AK, Gardner JL, han Chou I, Priebe NJ, Lisberger SG (2003)   Directional
856   anisotropies reveal a functional segregation of visual motion processing for perception
857   and action. *Neuron* 37:1001–1011.
858   Connolly M, Essen DV (1984) The representation of the visual field in parvicellular and
859   magnocellular layers of the lateral geniculate nucleus in the macaque monkey. *The*
860   *Journal of Comparative Neurology* 226:544–564.
861   Curado S, Anderson RM, Jungblut B, Mumm J, Schroeter E, Stainier DY (2007)
862   Conditional targeted cell ablation in zebrafish: A new tool for regeneration studies.
863   *Developmental Dynamics* 236:1025–1035.
864   Daniel PM, Whitteridge D (1961) The representation of the visual field on the cerebral
865   cortex in monkeys. *J. Physiol. (Lond.)* 159:203–221.
866   Darlot C, L?pez-Barneo J, Tracey D (1981)   Asymmetries of vertical vestibular
867   nystagmus in the cat. *Experimental Brain Research* 41-41.
868   Demer JL (1992) Mechanisms of human vertical visual-vestibular interaction. *Journal of*
869   *Neurophysiology* 68:2128–2146.
870   Douglass AD, Kraves S, Deisseroth K, Schier AF, Engert F (2008)   Escape behavior
871   elicited by single, channelrhodopsin-2-evoked spikes in zebrafish somatosensory
872   neurons. *Current Biology* 18:1133–1137.
873   Duncan RO, Boynton GM (2003)   Cortical magnification within human primary visual
874   cortex correlates with acuity thresholds. *Neuron* 38:659–671.
875   Ehrlich DE, Schoppik D (2017) Control of movement initiation underlies the development
876   of balance. *Current Biology* 27:334–344.
877   Esposito MS, Capelli P, Arber S (2014)   Brainstem nucleus MdV mediates skilled
878   forelimb motor tasks. *Nature* 508:351–356.
879   Favilla M, Ghelarducci B, Noce AL, Starita A (1983) EMG responses of the vertical eye
880   muscles to dynamic and static natural vestibular stimulation about different axes in
881   alert rabbits. *Brain Research* 280:277–286.
882   Goolish EM, Okutake K (1999) Lack of gas bladder inflation by the larvae of zebrafish in
883   the absence of an air-water interface. *Journal of Fish Biology* 55:1054–1063.
884   Gottesman-Davis A, Peusner KD (2010)   Identification of vestibuloocular projection
885   neurons in the developing chicken medial vestibular nucleus. *Journal of Neuroscience*
886   *Research* 88:290–303.
887   Grasse KL, Lisberger SG (1992) Analysis of a naturally occurring asymmetry in vertical

20

888   smooth pursuit eye movements in a monkey. *Journal of Neurophysiology* 67:164–79.

889 Greaney MR, Privorotskiy AE, D'Elia KP, Schoppik D (2016) Extraocular motoneuron
890   pools develop along a dorsoventral axis in zebrafish, *Danio rerio*.   *Journal of*
891   *Comparative Neurology* 525:65–78.

892 Hansson BS, Stensmyr MC (2011) Evolution of insect olfaction. *Neuron* 72:698–711.

893 Harrison TC, Murphy TH (2014)   Motor maps and the cortical control of movement.
894   *Current Opinion in Neurobiology* 24:88–94.

895 Higashijima S, Hotta Y, Okamoto H (2000)   Visualization of cranial motor neurons in
896   live transgenic zebrafish expressing green fluorescent protein under the control of the
897   islet-1 promoter/enhancer. *Journal of Neuroscience* 20:206–218.

898 Highstein SM, Holstein GR (2006) The anatomy of the vestibular nuclei In *Progress in*
899   *Brain Research*, pp. 157–203. Elsevier.

900 Iwamoto Y, Kitama T, Yoshida K (1990a)   Vertical eye movement-related secondary
901   vestibular neurons ascending in medial longitudinal fasciculus in cat i. firing properties
902   and projection pathways. *Journal of Neurophysiology* 63:902–917.

903 Iwamoto Y, Kitama T, Yoshida K (1990b)   Vertical eye movement-related secondary
904   vestibular neurons ascending in medial longitudinal fasciculus in cat. ii. direct
905   connections with extraocular motoneurons. *Journal of Neurophysiology* 63:918–935.

906 Kaas JH (1997)   Topographic maps are fundamental to sensory processing.   *Brain*
907   *Research Bulletin* 44:107–112.

908 Kay JN, Finger-Baier KC, Roeser T, Staub W, Baier H (2001)   Retinal ganglion cell
909   genesis requires lakritz, a zebrafish atonal homolog. *Neuron* 30:725–736.

910 Ke SR, Lam J, Pai DK, Spering M (2013)   Directional asymmetries in human smooth
911   pursuit eye movements. *Investigative Opthalmology & Visual Science* 54:4409.

912 Knudsen EI, Lac S, Esterly SD (1987) Computational maps in the brain. *Annual Review*
913   *of Neuroscience* 10:41–65.

914 Kramer DL, McClure M (1982) Aquatic surface respiration, a widespread adaptation to
915   hypoxia in tropical freshwater fishes. *Environmental Biology of Fishes* 7:47–55.

916 Kuypers HGJM (2011)   Anatomy of the descending pathways   In
917   *Comprehensive Physiology*, pp. 597–666. Wiley-Blackwell.

918 Lacoste AM, Schoppik D, Robson DN, Haesemeyer M, Portugues R, Li JM, Randlett O,
919   Wee CL, Engert F, Schier AF (2015) A convergent and essential interneuron pathway
920   for mauthner-cell-mediated escapes. *Current Biology* 25:1526–1534.

921 Lemon RN (2008)   Descending pathways in motor control.   *Annual Review*
922   *of Neuroscience* 31:195–218.

923 Levine AJ, Lewallen KA, Pfaff SL (2012)   Spatial organization of cortical and spinal
924   neurons controlling motor behavior. *Current Opinion in Neurobiology* 22:812–821.

925 Longair MH, Baker DA, Armstrong JD (2011)   Simple neurite tracer: open source
926   software for reconstruction, visualization and analysis of neuronal processes.
927   *Bioinformatics* 27:2453–2454.

928 Ma LH, Gilland E, Bass AH, Baker R (2010) Ancestry of motor innervation to pectoral fin
929   and forelimb. *Nature Communications* 1:1–8.

930 Marti S, Bockisch CJ, Straumann D (2006)   Asymmetric short-term adaptation of the
931   vertical vestibulo-ocular reflex in humans. *Experimental Brain Research* 172:343–350.

932 Maruyama M, Fushiki H, Yasuda K, Watanabe Y (2004)   Asymmetric adaptive gain
933   changes of the vertical vestibulo-ocular reflex in cats. *Brain Research* 1023:302–308.

934 Matsuo V, Cohen B (1984)   Vertical optokinetic nystagmus and vestibular nystagmus
935   in the monkey: Up-down asymmetry and effects of gravity.   *Experimental Brain*
936   *Research* 53.
937 McCrea RA, Strassman A, May E, Highstein SM (1987) Anatomical and physiological
938   characteristics of vestibular neurons mediating the horizontal vestibulo-ocular reflex of
939   the squirrel monkey. *The Journal of Comparative Neurology* 264:547–570.
940 Mo W, Chen F, Nechiporuk A, Nicolson T (2010) Quantification of vestibular-induced eye
941   movements in zebrafish larvae. *BMC Neuroscience* 11:110.
942 Montgomery NM (1988) Projections of the vestibular and cerebellar nuclei in textit*Rana*
943   *pipiens*. *Brain, Behavior and Evolution* 31:82–95.
944 Nikolaou N, Lowe AS, Walker AS, Abbas F, Hunter PR, Thompson ID, Meyer MP (2012)
945   Parametric functional maps of visual inputs to the tectum. *Neuron* 76:317–324.
946 Pan YA, Choy M, Prober DA, Schier AF (2011)   Robo2 determines subtype-specific
947   axonal projections of trigeminal sensory neurons. *Development* 139:591–600.
948 Pan YA, Freundlich T, Weissman TA, Schoppik D, Wang XC, Zimmerman S, Ciruna B,
949   Sanes JR, Lichtman JW, Schier AF (2013) Zebrabow: multispectral cell labeling for
950   cell tracing and lineage analysis in zebrafish. *Development* 140:2835–2846.
951 Pasqualetti M, Diaz C, Renaud J, Rijli F, Glover J (2007) Fate-mapping the mammalian
952   hindbrain: Segmental origins of vestibular projection neurons assessed using
953   rhombomere-specific hoxa2 enhancer elements in the mouse embryo.   *Journal of*
954   *Neuroscience* 27:9670–9681.
955 Pavlova E, Deliagina T (2002) Responses of reticulospinal neurons in intact lamprey to
956   pitch tilt. *Journal of Neurophysiology* 88:1136–1146.
957 Pisharath H, Rhee JM, Swanson MA, Leach SD, Parsons MJ (2007)   Targeted
958   ablation of beta cells in the embryonic zebrafish pancreas using e. coli nitroreductase.
959   *Mechanisms of Development* 124:218–229.
960 Popratiloff A, Peusner KD (2007) Otolith fibers and terminals in chick vestibular nuclei.
961   *The Journal of Comparative Neurology* 502:19–37.
962 Puzdrowski RL, Leonard RB (1994)   Vestibulo-oculomotor connections in an
963   elasmobranch fish, the atlantic stingray, dasyatis sabina. *The Journal of Comparative*
964   *Neurology* 339:587–597.
965 Randlett O, Wee CL, Naumann EA, Nnaemeka O, Schoppik D, Fitzgerald JE, Portugues
966   R, Lacoste AMB, Riegler C, Engert F, Schier AF (2015) Whole-brain activity mapping
967   onto a zebrafish brain atlas. *Nature Methods* 12:1039–1046.
968 Rathelot JA, Strick PL (2009)   Subdivisions of primary motor cortex based
969   on cortico-motoneuronal cells. *Proceedings of the National Academy of*
970   *Sciences* 106:918–923.
971 Riley BB, Moorman SJ (2000)   Development of utricular otoliths, but not saccular
972   otoliths, is necessary for vestibular function and survival in zebrafish.   *Journal*
973   *of Neurobiology* 43:329–337.
974 Roberts R, Elsner J, Bagnall MW (2017) Delayed otolith development does not impair
975   vestibular circuit formation in zebrafish.   *Journal of the Association for Research in*
976   *Otolaryngology* 18:415–425.
977 Rombough P (2007) The functional ontogeny of the teleost gill: Which comes first, gas
978   or ion exchange?   *Comparative Biochemistry and Physiology Part A: Molecular &*
979   *Integrative Physiology* 148:732–742.

22

980 Schindelin J, Arganda-Carreras I, Frise E, Kaynig V, Longair M, Pietzsch T, Preibisch
981   S, Rueden C, Saalfeld S, Schmid B, Tinevez JY, White DJ, Hartenstein V, Eliceiri K,
982   Tomancak P, Cardona A (2012)   Fiji: an open-source platform for biological-image
983   analysis. *Nature Methods* 9:676–682.
984 Schoonheim PJ, Arrenberg AB, Bene FD, Baier H (2010) Optogenetic localization
985   and genetic perturbation of saccade-generating neurons in zebrafish. *Journal of*
986   *Neuroscience* 30:7111–7120.
987 Scott EK, Mason L, Arrenberg AB, Ziv L, Gosse NJ, Xiao T, Chi NC, Asakawa K,
988   Kawakami K, Baier H (2007)   Targeting neural circuitry in zebrafish using GAL4
989   enhancer trapping. *Nature Methods* .
990 Severi KE, Portugues R, Marques JC, O'Malley DM, Orger MB, Engert F (2014)
991   Neural control and modulation of swimming speed in the larval zebrafish.
992   *Neuron* 83:692–707.
993 Shenoy KV, Sahani M, Churchland MM (2013)   Cortical control of arm movements: A
994   dynamical systems perspective. *Annual Review of Neuroscience* 36:337–359.
995 Simoncelli EP (2003) Vision and the statistics of the visual environment. *Current Opinion*
996   *in Neurobiology* 13:144–149.
997 Simpson JI, Graf W (1981) Eye-muscle geometry and compensatory eye movements
998   in lateral-eyed and frontal-eyed animals.   *Annals of the New York Academy of*
999   *Sciences* 374:20–30.
1000 Smith FM, Croll RP (2011)   Autonomic control of the swimbladder.
1001   *Autonomic Neuroscience* 165:140–148.
1002 Steiger HJ, Büttner-Ennever J (1979)   Oculomotor nucleus afferents in the monkey
1003   demonstrated with horseradish peroxidase. *Brain Research* 160:1–15.
1004 Stewart WJ, McHenry MJ (2010) Sensing the strike of a predator fish depends on the
1005   specific gravity of a prey fish. *Journal of Experimental Biology* 213:3769–3777.
1006 Straka H (2003)   Differential spatial organization of otolith signals in frog vestibular
1007   nuclei. *Journal of Neurophysiology* 90:3501–3512.
1008 Straka H, Baker R (2013) Vestibular blueprint in early vertebrates. *Frontiers in Neural*
1009   *Circuits* 7.
1010 Straka H, Baker R, Gilland E (2001) Rhombomeric organization of vestibular pathways
1011   in larval frogs. *The Journal of Comparative Neurology* 437:42–55.
1012 Straka H, Fritzsch B, Glover JC (2014) Connecting ears to eye muscles: Evolution of a
1013   'simple' reflex arc. *Brain, Behavior and Evolution* 83:162–175.
1014 Suwa H, Gilland E, Baker R (1996) Segmental organization of vestibular and reticular
1015   projections to spinal and oculomotor nuclei in the zebrafish and goldfish.   *The*
1016   *Biological Bulletin* 191:257–259.
1017 Suwa H, Gilland E, Baker R (1999)   Otolith ocular reflex function of the tangential
1018   nucleus in teleost fish. *Annals of the New York Academy of Sciences* 871:1–14.
1019 Szentágothai J (1964) Pathways and synaptic articulation patterns connecting vestibular
1020   receptors and oculomotor nuclei   In *The Oculomotor System*, pp. 205–223. Hoeber
1021   Medical Division, Harper and Row.
1022 Tawk M, Bianco IH, Clarke JDW (2009) Focal electroporation in zebrafish embryos and
1023   larvae In *Methods in Molecular Biology*, pp. 145–151. Humana Press.
1024 Thiele TR, Donovan JC, Baier H (2014)   Descending control of swim posture by a
1025   midbrain nucleus in zebrafish. *Neuron* 83:679–691.

1026   Tomko D, Wall C, Robinson F, Staab J (1988)   Influence of gravity on cat vertical
1027   vestibulo-ocular reflex. *Experimental Brain Research* 69.
1028   Torres B, Fernández S, Rodríguez F, Salas C (2008) Distribution of neurons projecting
1029   to the trochlear nucleus in goldfish *Carassius auratus*.   *Brain, Behavior and*
1030   *Evolution* 45:272–285.
1031   Torres B, Pastor AM, Cabrera B, Salas C, Delgado-García JM (1992)
1032   Afferent
1033   s to the oculomotor nucleus in the goldfish (carassius auratus) as revealed by
1034   retrograde labeling with horseradish peroxidase.   *The Journal of Comparative*
1035   *Neurology* 324:449–461.
1036   Torres-Torrelo J, Rodríguez-Rosell D, Nunez-Abades P, Carrascal L, Torres B (2012)
1037   Glutamate modulates the firing rate in oculomotor nucleus motoneurons as a function
1038   of the recruitment threshold current. *The Journal of Physiology* 590:3113–3127.
1039   Uchino Y, Hirai N, Suzuki S (1982)   Branching pattern and properties of vertical-
1040   and horizontal-related excitatory vestibuloocular neurons in the cat.   *Journal of*
1041   *Neurophysiology* 48:891–903.
1042   Uchino Y, Sato H, Zakir M, Kushiro K, Imagawa M, Ogawa Y, Ono S, Meng H, Zhang
1043   X, Katsuta M, Isu N, Wilson V (2001)   Commissural effects in the otolith system.
1044   *Experimental Brain Research* 136:421–430.
1045   Urasaki A, Morvan G, Kawakami K (2006) Functional dissection of the tol2 transposable
1046   element identified the minimal cis-sequence and a highly repetitive sequence in the
1047   subterminal region essential for transposition. *Genetics* 174:639–649.
1048   Wang WC, McLean DL (2014) Selective responses to tonic descending commands by
1049   temporal summation in a spinal motor pool. *Neuron* 83:708–721.
1050   Wentzel P, Zeeuw CD, Holstege J, Gerrits N (1995) Inhibitory synaptic inputs to
1051   the oculomotor nucleus from vestibulo-ocular-reflex-related nuclei in the rabbit.
1052   *Neuroscience* 65:161–174.
1053   Xu X, Collins CE, Khaytin I, Kaas JH, Casagrande VA (2006) Unequal representation
1054   of cardinal vs. oblique orientations in the middle temporal visual area. *Proceedings of*
1055   *the National Academy of Sciences* 103:17490–17495.
1056   Yamamoto M, Shimoyama I, Highstein S (1978)   Vestibular nucleus neurons
1057   relaying excitation from the anterior canal to the oculomotor nucleus.   *Brain*
1058   *Research* 148:31–42.
1059   Zhang F, Wang LP, Brauner M, Liewald JF, Kay K, Watzke N, Wood PG, Bamberg E,
1060   Nagel G, Gottschalk A, Deisseroth K (2007) Multimodal fast optical interrogation of
1061   neural circuitry. *Nature* 446:633–639.
1062   Zolessi FR, Poggi L, Wilkinson CJ, Chien CB, Harris WA (2006)   Polarization and
1063   orientation of retinal ganglion cells *in vivo*. *Neural Development* 1:2.
1064
1065
1066
1067
1068
1069
1070
1071
1072
1073

1074
1075
1076
1077 **Figure 1:** Vestibular nucleus neurons labeled in Tg(-6.7FRhcrtR:gal4VP16). A, The expression
1078 pattern of Tg(-6.7FRhcrtR:gal4VP16); Tg(UAS-E1b:Kaede)s1999t (purple) is shown as a
1079 horizontal maximum intensity projection (MIP), with one vestibular neuron,
1080 co-labeled by focal electroporation of gap43-EGFP (white). Arrows point to the tangential ($_T$
1081 VN) and medial vestibular nuclei ($_M$VN) and the medial longitudinal fasciculus (MLF).
1082 Inset schematic of a dorsal view of a larval zebrafish, with a magenta rectangle indicating
1083 the location of the image. Scale 50 μm B-C, Horizontal (B) and sagittal (C) MIP of vestibular
1084 neurons in Tg(-6.7FRhcrtR:gal4VP16);Tg(UAS-KillerRed) (purple);Tg(isl1:GFP) (green, image
1085 gamma = 0.5) showing cranial motoneuron somata from nIII/nIV, nV, and nVII (green text).
1086 Arrows highlight neurons in the vestibular nuclei (VN) and the MLF. Scale 50 μm. D-F, Close-up
1087 of white boxed region in 1C, showing major branch patterns of vestibular neuron axon fascicle
1088 (purple) relative to extraocular motoneurons (green). 1D shows motoneurons from Tg(isl1:GFP)
1089 (green) in nIV (magenta arrow), superior rectus motoneurons of nIII
1090 (cyan arrow) and the midbrain/hindbrain boundary (white dotted line). 1E shows branches of
1091 the vestibular neuron axon fascicle (purple), emerging from the MLF (white arrow) in
1092 Tg(-6.7FRhcrtR:gal4VP16);Tg(UAS-KillerRed), projecting to nIV (magenta arrow) and nIII
1093 (cyan arrow). F, merge of 1D-1E. Scale 20 μm. G-I, Broad and close-up views of vestibular
1094 neuron axonal projection (purple) to nIII cell bodies (green), taken at the horizontal plane
1095 delineated by the cyan dotted line in 1F, superior rectus (SR) motoneurons (nIII) encircled in
1096 cyan. Cyan arrows in 1G localize close-ups in 1H and 1I. Scale 10 μm J-L, Broad and close-up
1097 view of vestibular neuron axonal projection (purple) to nIV cell bodies (green), taken at the
1098 horizontal plane delineated by the magenta dotted line in 1F, superior oblique (SO)
1099 motoneurons (nIV, green) encircled in magenta. Arrows in 1J point to close-up in 1K and 1L.
1100 Scale 10 μm.
1101
1102
1103
1104
1105
1106
1107
1108
1109
1110
1111
1112
1113
1114
1115
1116
1117
1118 **Figure 2:** Projections from singly labeled vestibular nucleus neurons. A, Horizontal MIP
1119 of a single vestibular neuron labeled with UAS-ChR2(H134R)-EYFP (purple) in
1120 Tg(-6.7FRhcrtR:gal4VP16);Tg(isl:GFP) (green). Gamma = 0.5 to highlight the sparse
1121 label. Scale 100 μm. Pink triangle refers to the data in Figure 7D. 23/27 neurons studied
1122 projected similarly. B, Sagittal MIP of the neuron in Figure 2A highlighting nIII (cyan arrow), nIV
1123 (magenta arrow), and projection to nIV (white arrow). Scale 20 μm. C, Horizontal MIP of nIV
1124 (green cell bodies in dotted magenta outline) from 2A, Vestibular neuron projection (purple,
1125 white arrow) Scale 10 μm. D, Horizontal MIP of nIII (green cell bodies in dotted cyan outline)

25

1126   with no proximal vestibular neuron projection (purple) . E, Sagittal MIP of a single axon
1127   expressing 14xUAS-E1b:hChR2(H134R)-EYFP (purple)
1128   in Tg(-6.7FRhcrtR:gal4VP16);Tg(isl1:GFP) (green); Tg(atoh7:gap43-RFP)(cyan) fish. Expression
1129   of bright EGFP bleeds into the purple channel, making the cell bodies white. nIV (magenta
1130   arrow) nIII (cyan arrow) and the vestibular neuron projection to SR motoneurons in nIII (white
1131   arrow). Scale 20 μm. 4/27 neurons projected similarly, exclusively to nIII.
1132   F, Horizontal MIP of nIII (cells in blue outline) from 2e, purple projections from vestibular neuron
1133   (white arrow). Scale 10 μm G, Horizontal MIP of nIV (cells in magenta outline) from 2e with no
1134   purple vestibular neuron projection. Scale 10 μm.
1135
1136
1137
1138
1139
1140
1141
1142
1143
1144
1145
1146
1147
1148
1149
1150
1151
1152
1153
1154
1155
1156
1157
1158   **Figure 3:** Tracings of two vestibular nucleus neurons from a single fish at two developmental
1159   timepoints. A, Horizontal (top) and sagittal (bottom) projections of two traced neurons taken from
1160   the same fish imaged at 5 days post-fertilization. The magenta trace shows the characteristic
1161   projection to the nIV motoneuron pool (magenta arrows) while the green neuron does not. B,
1162   Same two neurons traced in the same fish, at 11 days post-fertilization. The same projection to
1163   nIV is visible in the magenta tracing (magenta arrow). Scale bars are 100 μm.
1164
1165
1166
1167
1168
1169
1170
1171
1172
1173
1174
1175
1176
1177
1178
1179
1180

26

1181
1182
1183
1184
1185
1186 **Figure 4:** Vestibular nucleus neurons show synaptophysin-positive puncta on their
1187 motoneuron targets. A, Sagittal MIP of a labeled SO motoneuron (magenta arrow) in
1188 green and the purple synaptic puncta labeled in Tg(-6.7FRhcrtR:gal4VP16);
1189 Tg(5xUAS:sypb-GCaMP3). Dotted lines indicate the planes in 4B-4C, scale 20 μm. B,C,
1190 Close-up slice of the motoneuron somata in 4A with puncta (magenta arrow), scale 10
1191 μm. D, Close-up of a retrogradely labeled SR motoneuron soma (green) with visible purple
1192 puncta (cyan arrow), Scale 10 μm. E, Close-up of the dendrites of SR motoneurons (green) with
1193 visible purple puncta (cyan arrow). Scale 10 μm.
1194
1195
1196
1197
1198
1199
1200
1201
1202
1203
1204
1205
1206
1207
1208
1209
1210
1211
1212
1213
1214 **Figure 5:** Vestibular nucleus neurons labeled in Tg(-6.7FRhcrtR:gal4VP16) are necessary for
1215 both nose-up and nose-down gaze stabilization. A, Horizontal MIP of vestibular and control
1216 neurons (nVII) in rhombomeres 4-8 in Tg(-6.7FRhcrtR:gal4VP16); Tg(UAS-E1b:Kaede)s1999t;
1217 Tg(isl1:GFP) fish before and after targeted photo-ablation of vestibular neuron cell bodies.
1218 Gamma = 0.5 to highlight dim signal, colors indicates depth
1219 over $\sim 150 \mu m$, white arrows point to the general region of targeted cell bodies in either the
1220 vestibular nuclei (top row) or the facial nucleus (nVII), scale bar = 150 μm. For anatomical
1221 localization compare to the right side of Figure 1B. B, Vestibulo-ocular reflex gain pre- and
1222 post-ablation of vestibular neurons. C, Vestibulo-ocular reflex gain pre- and post-ablation of
1223 facial nucleus neurons. D, Vestibulo-ocular reflex gain wild-type siblings (WT) and fish
1224 with pharmacogenetic (nitroreductase, "nfsb") and optogenetic ablation (Killer-Red, "KR") of
1225 neurons in Tg(-6.7FRhcrtR:gal4VP16)
1226
1227
1228
1229
1230
1231
1232
1233

27

1234
1235
1236
1237
1238
1239
1240
1241
1242
1243
1244
1245
1246 **Figure 6:** The simplified neural circuit underlying the ocular response to pitch and roll tilts.
1247 Cyan = nose down, magenta = nose up channels. A, Wiring diagram of one hemisphere of
1248 the excitatory vestibulo-ocular circuit showing utricular hair cells (cyan/magenta),
1249 stato-acoustic ganglion (SAG), central vestibular neurons (VN, cyan and magenta),
1250 extraocular motoneuron pools in nIII (SR, IR, IO) and nIV (SO). B, During a roll tilt to the fish's
1251 left, the left utricle hair cells (cyan/magenta) are activated, causing co-contraction of superior
1252 (SO/SR) eye muscles ipsilateral to the activated utricle, and inferior (IO/IR) muscles
1253 contralateral to the activated utricle. C, Utricular hair cells sensitive to nose-up
1254 pitch tilts (magenta) ultimately activate only vestibular neurons that project to both nIII and nIV,
1255 activating SO (contralateral) and IR (ipsilateral). D, Utricular hair cells sensitive to
1256 nose-down pitch tilts (cyan) ultimately activate vestibular neurons that project to exclusively to nIII,
1257 activating SR (contralateral) and IO (ipsilateral).
1258
1259
1260
1261
1262
1263
1264
1265
1266
1267
1268
1269
1270
1271
1272
1273
1274
1275
1276
1277
1278 **Figure 7:** Activating vestibular nucleus neurons generates downward eye rotations. A, Peak
1279 eye rotation as a function of blue light duration. Positive values indicate eyes-down rotations
1280 (magenta arrow), negative values are eyes-up (cyan arrow). ChR2+ fish in black,
1281 ChR2- siblings in gray. Points are median ± median absolute deviation. B, Evoked eye
1282 rotation in time. Gray lines are individual fish, black lines the median of pre-lesion data,
1283 red lines are the same fish after photoablation of ChR2+ vestibular neurons. Stimulus (100 ms) in
1284 blue. C, Gray lines are the average responses from individual fish with pan-neuronal expression.
1285 Black is the median across fish, stimulus (100 ms) in blue. The trace with a downward lobe
1286 reflects a non-torsional component; video of this fish is shown as Movie M4. D, Evoked ocular

28

1287   rotations from sparsely labeled fish as a function of ChR2+ expression (MLF fluorescence). Fish
1288   with discriminable vestibular neurons shown as black dots, without in green. The pink triangle
1289   corresponds to the fish in Figure 2A
1290
1291
1292
1293
1294
1295
1296
1297
1298
1299
1300
1301
1302
1303
1304
1305
1306
1307
1308
1309
1310
1311
1312   **Figure 8:**   A, Model schematic B, One simulation of the model for two different population sizes,
1313   180 neurons (magenta) and 30 neurons (cyan). The first column shows the vestibular neuron
1314   activity as a spike raster plot and the input function (black). The second column shows the
1315   motoneuron spikes. For display, half the generated spikes are shown in each raster. C, The
1316   "Output strength" (average firing rate) of the post-synaptic neurons as a function of the
1317   population size (rows) and number of inputs per motoneuron (columns). D, The "Encoding
1318   fidelity" (variance explained, R) in the input rate function by the summed post-synaptic output.
1319
1320
1321
1322
1323
1324
1325
1326
1327
1328
1329
1330
1331
1332
1333
1334
1335
1336
1337
1338
1339
1340
1341
1342

1343 **Figure 9:** Early ablations of vestibular neurons leave fish unable to inflate their swim bladders.
1344 a) Tg(-6.7FRhcrtR:gal4VP16); Tg(14xUAS-E1b:hChR2(H134R)-EYFP); mitfa -/- fish swimming
1345 in a cuvette in the dark at 144hpf. Red arrows point to swim bladders. b) Sibling fish where the
1346 vestibular neurons in these fish were photoablated at 72hpf, before swim bladder inflation. Note
1347 the absence of a swim bladder, evaluated here at 144hpf.
1348 Images are taken from Movies M6-M7.
1349
1350
1351
1352
1353
1354
1355
1356
1357
1358
1359
1360
1361
1362
1363

1364 # Movie Legends

1365 ## Movie M1: Reconstruction of an nIV-projecting neuron.

1366 Data is taken from the same confocal stack shown in Figure 2A-2D. The neuron
1367 is shown in black, colored spheres represent the center locus of cell bodies of nIV
1368 (magenta) and nIII (cyan) cranial motoneurons. The movie begins with the neuron in
1369 a horizontal orientation, rotates 90° along the x axis until it is sagittal, and then rotates
1370 90° along the y axis such that the viewer looks caudally down the long axis of the fish
1371 towards the tail. The large projection to nIV is clearly visible. Scale bar is 25 μm for all
1372 three axes.
1373

1374 ## Movie M2: Reconstruction of an nIII-projecting neuron.

1375 Data is taken from the same confocal stack shown in Figure 2E-2G. The neuron
1376 is shown in black, colored spheres represent the center locus of cell bodies of nIV
1377 (magenta) and nIII (cyan) cranial motoneurons. The movie begins with the neuron in a
1378 horizontal orientation, rotates 90° along the x axis until it is sagittal, and then rotates 90°
1379 along the y axis such that the viewer looks caudally down the long axis of the fish
1380 towards the tail. The terminal arbors of this neuron are considerably more restricted
1381 than the neuron in M2, and bypass nIV, terminating in nIII. Scale bar is 25 μm for all
1382 three axes.

1383 ## Movie M3: A sample eye movement evoked by a blue light flash in
1384 wild-type fish.

1385 The left eye of a wild-type fish responding to a flash of blue light. Green box reflects
1386 the realtime estimate of the eye's rotation. Movie is 4 sec, with a 100msec flash after 2
1387 sec. For clarity, the original video was enlarged 4x and slowed down 4-fold (200Hz
1388 acquisition, 50Hz playback).
1389

30

Movie M4: A sample eye movement evoked by a blue light flash in fish expressing channelrhodopsin in vestibular neurons.

The left eye of a Tg(-6.7FRhcrtR:gal4VP16); Tg(14xUAS-E1b:hChR2(H134R)-EYFP); atoh7th241/th241; Tg(atoh7:gap43-RFP) fish responding to a flash of blue light. Gray box reflects the realtime estimate of the eye's rotation. Movie is 3.6sec long, with a 100msec flash at 1.2sec indicated by a cyan circle.

Movie M5: A sample eye movement evoked in a fish with pan-neuronal   channelrhodopsin.

The left eye of a Tg(s1101t:gal4); Tg(14xUAS-E1b:hChR2(H134R)-EYFP); atoh7th241/th241; Tg(atoh7:gap43-RFP) fish responding to a flash of blue light. Green box reflects the realtime estimate of the eye's rotation. Movie is 4 sec, with a 100ms flash after 2 sec. For clarity, the original video was enlarged 4x and slowed down 4-fold (200Hz acquisition, 50Hz playback). Note the rapid and transient change in the angle of the green square at the initiation of the evoked eye movement. This reflects the tracker failing due to the nasal-ward component of the eye's contraction. After the brief failure of the tracker, it recovers, and the downward torsional component of the eye movement becomes visible.
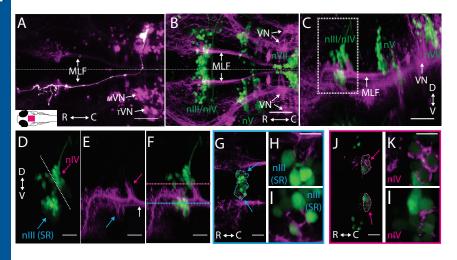

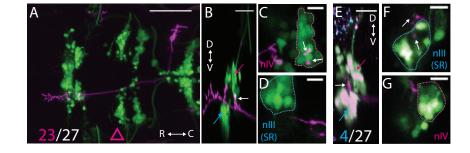**Movie M6: Fish without vestibular neurons swimming in a cuvette.**

Tg(-6.7FRhcrtR:gal4VP16); Tg(14xUAS-E1b:hChR2(H134R)-EYFP); mitfa -/- fish swimming in a cuvette. Vestibular neurons in these fish were photoablated at 72hpf, before swim bladder inflation. Note the absence of a swim bladder, evaluated here at 144hpf. These fish are siblings of the fish in Movie M7.
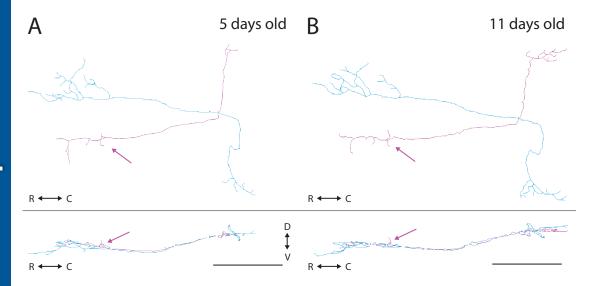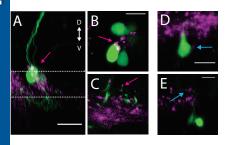

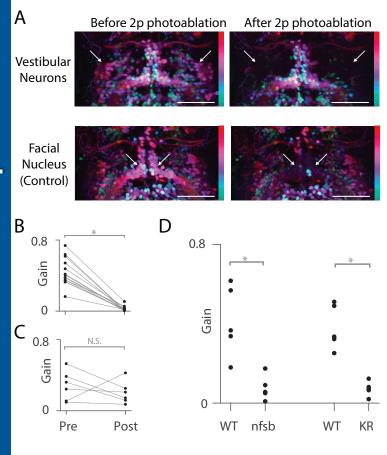**Movie M7: Fish swimming in a cuvette.**

Tg(-6.7FRhcrtR:gal4VP16); Tg(14xUAS-E1b:hChR2(H134R)-EYFP); mitfa -/- fish filmed at 144hpf. Note the presence of a swim bladder. These fish are siblings of the fish in Movie M6.

A
5 days old

B
11 days old

R ←→ C

R ←→ C

D
↕
V

R ←→ C

R ←→ C

A

Before 2p photoablation   After 2p photoablation

Vestibular
Neurons

Facial
Nucleus
(Control)

B

C

Pre   Post

D

WT   nfsb   WT   KR

A

B
Leftward roll

C
Nose-up pitch tilt

D
Nose-down pitch tilt

A ChR2+
   ChR2-
Eye rotation (°)
7
0
10   10³   10⁵
Stimulus (μsec)

B Pre-ablation
   Post-ablation
7
0
0   1   2
Time (sec)

C
Eye rotation (°)
5
0
-5
0   0.25   0.5
Time (sec)

D
1.25
0
-1
Sparse VN
Sparse other
0   6
MLF fluorescence

A

1. Input   2. Transformation   3. Integration   4. Output

Afferents   Vestibular Neurons   Motoneurons   Eyes

B

Vestibular Motoneuron

C Output strength Hz

# of vestibular neurons

30
70
140
180

6 14 22 30
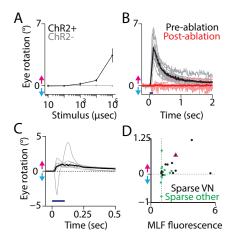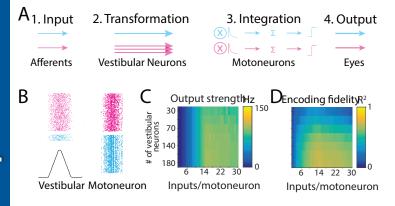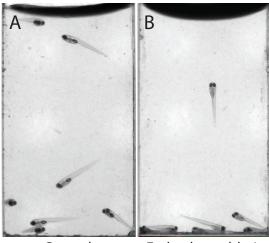Inputs/motoneuron

150

0

D Encoding fidelity R²

6 14 22 30
Inputs/motoneuron

1

0

Control   Early photoablation